

# Investigation of charge correlations and determination of effective Coulomb interaction in low dimensional doped quantum antiferromagnets

**Suraka Bhattacharjee<sup>1</sup> and Ranjan Chaudhury<sup>1,2</sup>**

<sup>1</sup>Department of Condensed Matter Physics and Material Sciences

S.N. Bose National Centre for Basic Sciences

Saltlake, Sector-III, Block-JD, Kolkata-700106, India

<sup>2</sup>Department of Physics

Ramakrishna Mission Vivekananda Educational and Research Institute  
Belur-711202, India

Email- <sup>1</sup>surakabhatta@bose.res.in, <sup>1,2</sup>ranjan@bose.res.in,  
ranjan.chowdhury@rkmvu.ac.in

June 30, 2022

## Abstract

Expressions for generalized charge stiffness constant for low dimensional hole doped quantum antiferromagnets are derived corresponding to the t-J-like models, in both strong and weak correlation limits. A detailed comparison highlights that the charge and spin couplings show very similar behaviour in the over-doped region and a completely different trend in the lower doping regimes. Based on the results, a phase diagram is drawn, showing the regions of different charge interactions. Moreover, a detailed analysis of our results with those from experimental and other theoretical approaches established the equivalence of generalized charge stiffness constant and effective Coulomb interaction. The fall in charge stiffness thus implies the reduction in magnitude of effective Coulomb repulsion between charge carriers, enhancing the possibility of fermionic pairing, provided some other attraction producing mechanism is present. Therefore, it is also established that t-J-like models themselves can not produce conventional momentum-space based superconducting pairing on their own.

# 1 Introduction

Most of the cuprate superconductors are known to exhibit many characteristicistic phases, supported by consistent experimental evidences [1, 2, 3]. The spin dynamics plays an important role in studying the magnetic behaviour of the different phases. The interaction between the charge degrees of freedom, in effect to the Coulomb potential, are also important in determining the pairing possibility in strongly correlated doped magnetic systems [4]. The study of spin and charge correlations in the itinerant phases of doped cuprates involves the Cu and the O bands [5, 6]. However, various theoretical techniques were used to reduce the two band Hamiltonian to the single-band t-J model, which is extensively used in investigating the correlations in the doped antiferromagnets in the under-doped regime [7, 8, 9].

The magnetic interaction in 2D systems was studied using many theoretical approaches including Mori's projection technique based on two-time thermodynamic Green's function and Variational Monte Carlo simulations [10, 11, 12, 13, 14]. On the other hand, the 1D t-J model is exactly solvable using Bethe Ansatz at specific values of  $J/t$  [15, 16]. The Density Matrix Renormalization Group (DMRG) and Transfer Matrix Renormalization Group (TMRG) techniques have also been used to find the spin correlations away from the super-symmetric points [17, 18]. In our recent papers, we have developed a non-perturbative quantum mechanical approach to determine the spin correlations in both 2D and 1D doped antiferromagnets, on the basis of generalized spin stiffness constant corresponding to the t-J model [19, 20]. Our results in 1D lead to a very interesting consequence regarding the formation of a new type of spin-spin coupling as doping increases, which is totally distinct from the original antiferromagnetic coupling seen in the insulating and under-doped phases [20]. Our novel prediction was further supported by other experimental and theoretical results [20].

Beside the spin correlations, there were some earlier works to find the charge correlations and effective Coulomb interaction in the systems. These works include the determination of the inverse dielectric function, involving the standard many body formalism in a Fermi liquid [21]. The total free energy used in the calculation comprises of the Hartree-like term and the exchange correlation contributions [21]. It was found that the Coulomb interaction thus calculated from the inverse of dielectric function, can even change sign and turn attractive if the spin susceptibility is larger than a threshold value [21]. This can trigger the possibility of pairing in some of the doped antiferromagnetic systems. However, the above technique could not determine the charge coupling in strongly correlated phases of the systems, where the double fermionic occupancy on each site is disallowed.

There were some other attempts to find the local charge stiffness tensor ( $D_{\alpha\beta}$ ) as the response of the system to any change in boundary condition [22]. The component  $D_{\alpha\alpha}$  was used to find the optical mass and was shown to be directly proprtional to the Drude weight [22]. But the charge stiffness constants, calculated applying the Lanczos algorithm, were at discrete values of hole concentrations [22, 23]. Again,

the Drude weight calculated by exact diagonalization technique in Hubbard cluster shows an increase in the lower doping regime, where the interacting holes are considered as the major carriers [24]. Further in the over-doped regime, the weakly interacting electrons take the role of the major carriers and the Drude weight falls in magnitude [25]. Moreover, the dynamical conductivity derived based on the memory function technique in terms of the Hubbard operators, was found to be proportional to doping concentration [26]. Thus the result shows that increase in  $\delta$  signifies the enhanced mobility of the carriers, resulting from the decreased Coulomb interaction between the charges. [26].

In this paper, our objective is to determine the effective interaction between the mobile charge degrees of freedom in the doped antiferromagnetic systems and explore various consequences arising from this. The doping dependence of charge-charge coupling is studied in terms of the evolution of generalized charge stiffness constant with doping concentration. In the strongly correlated under-doped regime, we have compared our derived results of charge stiffness with the experimentally extracted effective Coulomb interaction obtained from the imaginary part of conductivity measured on the layers of  $\text{La}_{2-x}\text{Sr}_x\text{CuO}_4$  [27]. However, in the weakly correlated over-doped regime, we have done a comparative study amongst the results obtained from theoretical approaches, we have used viz (i) t-J model model allowing double occupancies; (ii)  $t_1-t_2-t_3-J$  model; (iii) interacting high density electron gas and interacting band electrons [28, 29].

To summarize, we present here a non-perturbative quantum mechanical approach for determining the charge correlations and the effective Coulomb interaction between the mobile charge degrees of freedom in the low-dimensional doped quantum antiferromagnets. Based on our calculations, we have drawn a phase diagram showing the regimes with different coupling strengths for the charge degrees of freedom. We have also discussed its implications for superconducting pairing as well as possible formation of charge density wave in these systems.

## 2 Results and Comparisons

### 2.1 Calculational Formalism and Numerical Results for charge stiffness with t-J model

#### 2.1.1 Strongly correlated and with nearest neighbour hopping

The nearest neighbour t-J model Hamiltonian for strongly correlated electronic systems is [19, 20, 30]:

$$H_{t-J} = H_t + H_J \quad (1)$$

where  $H_t$  and  $H_J$  represents the hopping and exchange interactions involving nearest neighbour sites, respectively with restrictions on double occupancy at each site [19, 20, 29].

As was done earlier for generalized spin stiffness constant ( $\tilde{D}_s$ ), a similar kind of equation also holds for the generalized charge stiffness ( $\tilde{D}_c$ )[19, 20]

$$\tilde{D}_c = \tilde{D}_c^t + \tilde{D}_c^J \quad (2)$$

where  $\tilde{D}_c^t$  and  $\tilde{D}_c^J$  are the contributions to spin stiffness constant from kinetic energy and exchange energy respectively and are given by [19, 20]:

$$\tilde{D}_c^t = \lim_{\phi \rightarrow 0} \left( \frac{1}{2} \right) \frac{\delta^2 T}{\delta \phi^2} \quad (3)$$

and

$$\tilde{D}_c^J = \lim_{\phi \rightarrow 0} \left( \frac{1}{2} \right) \frac{\delta^2 E_J}{\delta \phi^2} \quad (4)$$

where  $\phi$  is the magnetic twist corresponding to the Peierls's phase  $\phi_\sigma$  arising from the presence of the vector potential  $\mathbf{A}(\vec{r})$ [19, 20]. The quantity  $\phi_\sigma$  has the following property for the spin symmetric case:

$$\phi_\downarrow = \phi_\uparrow = \phi \quad (5)$$

[This is unlike the spin asymmetric case, where we had used  $\phi_\downarrow = -\phi_\uparrow = \phi$  [19, 20, 30]]

We have evaluated the expectation values in the Gutzwiller state [19, 20, 30].

$$|\psi_G\rangle = \prod_l (1 - \alpha \hat{n}_{l\uparrow} \hat{n}_{l\downarrow}) |FS\rangle \quad (6)$$

where  $\alpha$  is the variational parameter deciding the amplitude for no-double occupancy of any site and  $|FS\rangle$  is the Fermi sea ground state [19, 20, 30]. At first we take  $\alpha=1$  for completely projecting out the doubly occupied sites.

$$|\psi_G\rangle_{NDOC} = \prod_l (1 - \hat{n}_{l\uparrow} \hat{n}_{l\downarrow}) \prod_{k\sigma}^F \sum_{ij} C_{i\sigma}^\dagger C_{j-\sigma}^\dagger e^{i(\vec{r}_i - \vec{r}_j) \cdot \vec{k}} |vac\rangle \quad (7)$$

where  $|vac\rangle$ , i, j and l have the usual meaning [30].

The exchange energy for the spin symmetric case ( see eq.(5)) can be written as [19, 20]

$$E_J = \left( \frac{zt_{eff}^2}{V_{eff}} \right) \frac{NDOC \langle \psi_G | H'_J | \psi_G \rangle_{NDOC}}{NDOC \langle \psi_G | \psi_G \rangle_{NDOC}} \quad (8)$$

where 'z' is the co-ordination number i.e., z=4 for 2-D and 2 for 1-D and

$$H'_J = \vec{S}_i \cdot \vec{S}_j - \frac{1}{4} n_i n_j \quad (9)$$

with  $_{NDOC}\langle\psi_G|\psi_G\rangle_{NDOC}$  being the normalization factor for the Gutzwiller state  $|\psi_G\rangle_{NDOC}$  [20].

Since  $E_J$  is  $\phi$  independent [see eq.(8)],

$$\tilde{D}_c^J = 0 \quad (10)$$

Thus  $\tilde{D}_c = \tilde{D}_c^t$  always.

Hence the exchange energy contribution to charge stiffness vanishes in the entire doping region. This may be physically interpreted as the interchange of spins has no effect on the carriers in terms of their charge responses.

The total charge stiffness is given by the kinetic energy contribution to charge stiffness ( $\tilde{D}_c^t$ ) and is derived taking the second order derivative of kinetic energy expectation value in the Gutzwiller state (see eqs.(3) and (7)).

In 2D,

$$\tilde{D}_c = (-t) \left[ \prod_{k_x, \sigma}^{k_F} 4\cos(k_x a)(1 - \delta)^2 - N_l \prod_{k_x, \sigma}^{k_F} 4\cos(k_x a)/N^2 \right] \quad (11)$$

(while the vector potential is applied in x-direction )

and for 1D,

$$\tilde{D}_c = (-t) \left[ \prod_{k, \sigma}^{k_F} 4\cos(ka)(1 - \delta)^2 - N_l \prod_{k, \sigma}^{k_F} 4\cos(ka)/N^2 \right] \quad (12)$$

where  $N_l = N(1 - \delta)$ ,  $N$  is the total number of sites and ‘ $\delta$ ’ is the doping concentration and the Fermi momentum  $k_F$  in 2-D has the form [19, 20, 30]:

$$k_F = \frac{\sqrt{2\pi(1 - \delta)}}{a} \quad (13)$$

and in 1-D:

$$k_F = (\pi/2a)(1 - \delta) \quad (14)$$

Here it can be noted that the form of  $\tilde{D}_c^t$  is similar to that of  $\tilde{D}_s^t$  in both one and two dimensions [19, 20, 30]. Hence following the same arguments described in our two previous papers [19, 20],  $\tilde{D}_c$  vanishes if at least one value of  $k_x$  in 2D (k in 1D) satisfies:

For 2D,

$$k_x a = \pi/2 \quad (15)$$

and for 1D

$$ka = \pi/2 \quad (16)$$

This condition can be satisfied only when  $k_F a = \pi/2$  [19, 20, 30]. Using the expressions for  $k_F$  (see eqs. (15,16)), one can get the vanishing conditions are  $\delta \rightarrow 1$  and  $\delta \leq 0.61$  for 2D model and at  $\delta \rightarrow 1$  and  $\delta \rightarrow 0$  for 1D [19, 20, 30]. For the vector potential applied in the x-direction, we get the value of  $\delta = \delta_c \approx 0.61$ , below which the charge stiffness remains zero in 2D.

The total charge stiffness constants derived for the strongly correlated  $\alpha=1$  case in 2D and 1D are plotted against  $\delta$  (see Figs.(1,2)) [19, 20]. In the plots, the total charge stiffness has been scaled down by the number of pairs of mobile holes in the system, to extract an equivalent stiffness corresponding to a pair of mobile charge carriers:

$$D_c = \tilde{D}_c / N_l C_2 \quad (17)$$

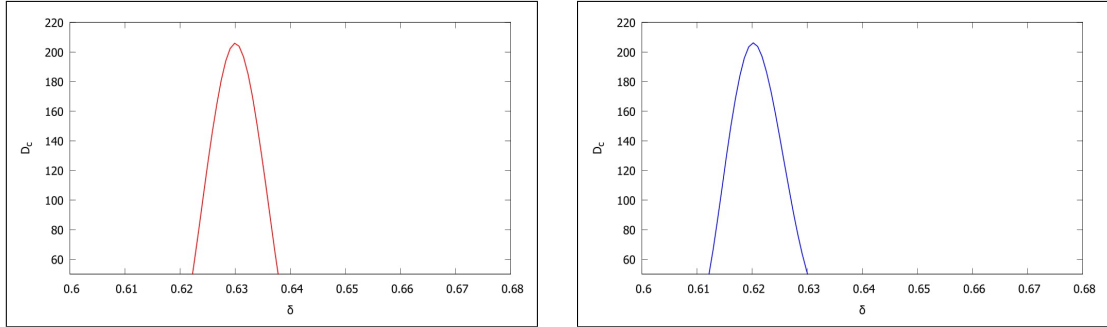


Figure 1:  $D_c$  vs.  $\delta$  in 2D: (a) lattice size=700x700; (b) lattice size=800x800

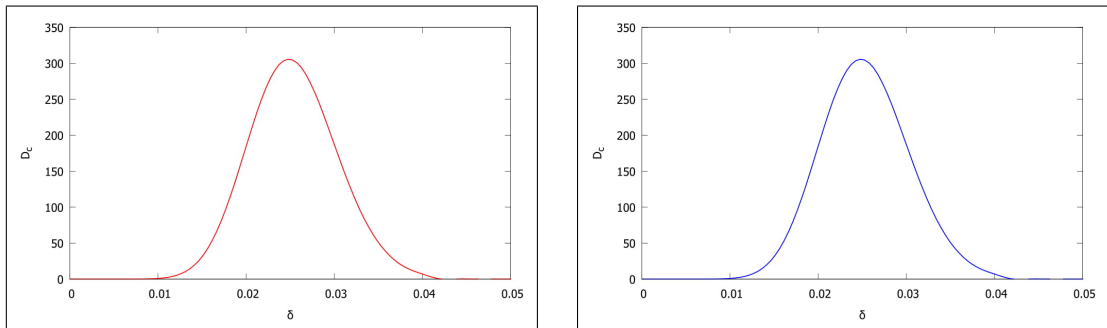


Figure 2:  $D_c$  vs.  $\delta$  in 1D: (a) lattice length=1800; (b) lattice length=1900

In 2D, the scaled charged stiffness constant vanishes upto the critical doping concentration  $\delta_c$ , followed by a sharp rise in  $D_c$ . The charge stiffness again falls drastically with further increase in doping concentration, giving rise to the appearance of a very sharp cusp-like peak in the over-doped region as shown in Figs.(1a,b). For the 1D model,  $D_c$  shows a maximum in the low doping region, and zero elsewhere (see Fig.(2a,b)).

### 2.1.2 Weakly correlated and with nearest neighbour hopping

Initially, we determine the charge stiffness in the normal Fermi liquid-like state with very small  $\alpha$ , using the nearest neighbour t-J model. For any value of  $\alpha$ , we get for 2D,

$$\tilde{D}_c = (-t) \left[ \prod_{k_x, \sigma}^{k_F} 4\cos(k_x a)(1 - \delta)^2 - \alpha N_l \prod_{k_x, \sigma}^{k_F} 4\cos(k_x a)/N^2 \right] \quad (18)$$

and in 1D,

$$\tilde{D}_c = (-t) \left[ \prod_{k, \sigma}^{k_F} 4\cos(ka)(1 - \delta)^2 - \alpha N_l \prod_{k, \sigma}^{k_F} 4\cos(ka)/N^2 \right] \quad (19)$$

Now, we consider the limiting case with  $\alpha=0$  i.e, the double occupancy is totally allowed on the sites and then the Gutzwiller state reduces to that of an ideal Fermi system:

$$|FS\rangle = \prod_{k\sigma}^{k_F} \sum_{ij} C_{i\sigma}^\dagger C_{j-\sigma}^\dagger e^{i(\vec{r}_i - \vec{r}_j) \cdot \vec{k}} |vac\rangle \quad (20)$$

Calculating the kinetic energy in this case also we get for 2D,

$$\tilde{D}_c = (-t) \prod_{k_x, \sigma}^{k_F} 4\cos(k_x a)(1 - \delta)^2 \quad (21)$$

In 1D,

$$\tilde{D}_c = (-t) \prod_{k, \sigma}^{k_F} 4\cos(ka)(1 - \delta)^2 \quad (22)$$

From eqs.(11-12) and (18-19), one can see that the magnitude of the total charge stiffness constant varies with  $\alpha$ ; however, the vanishing conditions remain the same for very small  $\alpha$  (including  $\alpha=0$ ) as well as very large  $\alpha$  including  $\alpha=1$ . This conclusion is essentially an artefact of ‘ $\alpha$ ’ being chosen as a free parameter in the calculation. Later, we have used the  $t_1-t_2-t_3-J$  model for more realistic analysis of the over-doped regime, since the higher neighbour hoppings are important in the highly doped regions. This is because of the weakening of the Coulomb interaction due to enhanced screening.

### 2.1.3 Weakly correlated and with higher neighbour hoppings

In the previous sub-section, we have derived the charge stiffness in the weakly correlated regime, considering only the nearest neighbour interaction. As we have already

stated that in the over-doped regime, the higher neighbour hoppings are also significant, so we have incorporated two higher neighbour terms in the t-J model.

The  $t_1-t_2-t_3-J$  model is given as:

$$H = -t_1 \sum_{\langle i,j \rangle, \sigma} C_{i\sigma}^\dagger C_{j\sigma} - t_2 \sum_{\langle\langle i,j \rangle\rangle, \sigma} C_{i\sigma}^\dagger C_{j\sigma} - t_3 \sum_{\langle\langle\langle i,j \rangle\rangle\rangle, \sigma} C_{i\sigma}^\dagger C_{j\sigma} + J \sum_{\langle i,j \rangle, \sigma} S_i \cdot S_j \quad (23)$$

where  $t_1$ ,  $t_2$  and  $t_3$  represent the first, second and third neighbour hopping amplitudes respectively.

In 2D,

$$\begin{aligned} \tilde{D}_c = & - \left[ \prod_{k_x, \sigma}^{k_F} 4 \{ (t_1) \cos(k_x a) + (t_2) \cos(2k_x a) + (t_3) \cos(3k_x a) \} (1 - \delta)^2 - \right. \\ & \left. \alpha N_l \prod_{k_x, \sigma}^{k_F} 4 \{ (t_1) \cos(k_x a) + (t_2) \cos(2k_x a) + (t_3) \cos(3k_x a) \} / N^2 \right] \quad (24) \end{aligned}$$

and in 1D,

$$\begin{aligned} \tilde{D}_c = & - \left[ \prod_{k, \sigma}^{k_F} 4 \{ (t_1) \cos(ka) + (t_2) \cos(2ka) + (t_3) \cos(3ka) \} (1 - \delta)^2 - \right. \\ & \left. \alpha N_l \prod_{k, \sigma}^{k_F} 4 \{ (t_1) \cos(ka) + (t_2) \cos(2ka) + (t_3) \cos(3ka) \} / N^2 \right] \quad (25) \end{aligned}$$

Putting  $\alpha=0$  eqs.(24,25) reduce to:

For two dimension,

$$\tilde{D}_c = - \prod_{k_x, \sigma}^{k_F} 4 \{ (t_1) \cos(k_x a) + (t_2) \cos(2k_x a) + (t_3) \cos(3k_x a) \} (1 - \delta)^2 \quad (26)$$

and for one dimension,

$$\tilde{D}_c = - \prod_{k, \sigma}^{k_F} 4 \{ (t_1) \cos(ka) + (t_2) \cos(2ka) + (t_3) \cos(3ka) \} (1 - \delta)^2 \quad (27)$$

The eqs.(24-27) show that the vanishing conditions for  $\tilde{D}_c$  corresponding to very small  $\alpha$  and  $\alpha=0$  in 2D are  $\delta \rightarrow 1$  and  $\delta \leq \delta_c$ , where  $\delta_c$  depends on the relative magnitudes of  $t_1$ ,  $t_2$  and  $t_3$ . For  $t_2=t_3=0$  with  $\alpha=0$ , the value of  $\delta_c$  becomes 0.61, which is exactly the same as the corresponding value of  $\delta_c$  obtained for the nearest neighbour t-J model. For 1D  $t_1-t_2-t_3-J$  model,  $D_c$  vanishes only at  $\delta \rightarrow 1$ , however,

the vanishing conditions for pure t-J model are retained for  $t_2=t_3=0$ . Thus it can be inferred that the zeros of  $\tilde{D}_c$  occur at the same value of doping concentration, when approached from the strongly correlated region or uncorrelated side. This may very well represent a point of possible quantum phase transition between two regions of constant stiffness separated by a sharp peak. The recent experimental observations from some of the doped correlated systems seem to have a strong link with this result of ours [31].

The plots of  $D_c$  for uncorrelated  $t_1-t_2-t_3-J$  model in two dimension, are presented in Fig.(3). The corresponding plots for 1D are given in Fig.(4). The values of  $t_2/t_1$  and  $t_3/t_1$  were determined by fitting the tight binding Fermi surfaces to the experimental results on  $\text{La}_{2-x}\text{Sr}_x\text{CuO}_4$  and  $\text{Bi}2212$  [32, 33]. The second neighbour hopping amplitude was found to be of opposite sign with respect to the first neighbour hopping. Here, we have done the calculations for a range of feasible values of  $t_2$  and  $t_3$  and presented a result for a few sets of  $t_2/t_1$  and  $t_3/t_1$ .

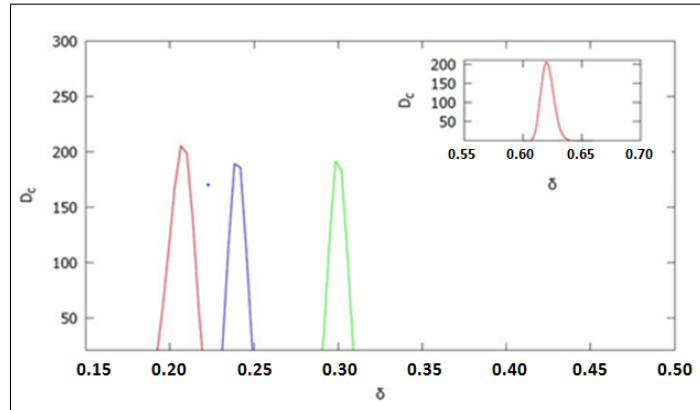


Figure 3:  $D_c$  vs.  $\delta$  for 2D  $t_1-t_2-t_3-J$  model, with  $\alpha=0$ ; (a)peak at  $\delta \sim 0.29$  ( $t_2=-0.53t_1, t_3=0.24t_1$ ) [green line]; (b)peak at  $\delta \sim 0.23$  ( $t_2=-0.52t_1, t_3=0.45t_1$ ) [blue line]; (c)peak at  $\delta \sim 0.19$  ( $t_2=-0.6t_1, t_3=0.56t_1$ ) [red line] [in the inset is shown  $D_c$  vs.  $\delta$  for  $t_2=t_3=0$ ; the peak is seen at  $\delta \sim 0.61$ ]

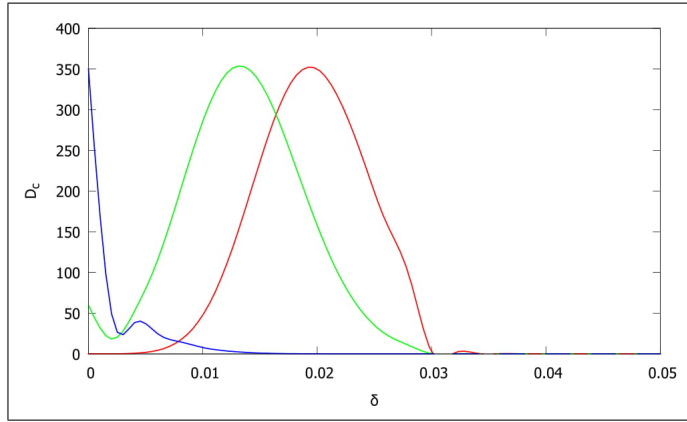


Figure 4:  $D_c$  vs.  $\delta$  for 1D  $t_1-t_2-t_3-J$  model, with  $\alpha=0$ ; (a)peak at  $\delta \sim 0.02$  ( $t_2=-0.01t_1, t_3=0.005t_1$ ) [red line]; (b)peak at  $\delta \sim 0.013$  ( $t_2=-0.02t_1, t_3=0.01t_1$ ) [green line]; (c)peak at  $\delta \rightarrow 0$  limit ( $t_2=-0.04t_1, t_3=0.02t_1$ ) [blue line]

The Fig.(3) shows that the maximum in  $D_c$  shifts to the optimal doping region for range of values of  $t_2/t_1$  and  $t_3/t_1$ . Again, the peak gradually shifts to further lower doping concentration for relatively higher magnitudes of second and third neighbour hopping amplitudes ( $|t_2|$  and  $|t_3|$ )(see Fig.(3)).

Similarly in 1D too, the peak in  $D_c$  shifts to very low doping regime as  $|t_2|$  and  $|t_3|$  are enhanced and the position of the peak reaches  $\delta \rightarrow 0$  limit at  $t_2 \approx -0.04t_1$  and  $t_3 \approx 0.02t_1$  (see (Fig.(4))).

#### 2.1.4 Calculation of effective interaction from dielectric function approach

In the over-doped region, the electronic charge correlation weakens substantially and the system exhibits normal Fermi liquid-like behaviour. In this weakly correlated electronic system, the effective static Coulomb interaction between the mobile charge carriers can be determined using the dielectric function approach [28, 33, 34].

Initially, one determines the dynamic dielectric function and then take  $\omega \rightarrow 0$  limit for extraction of the static Coulomb interaction. The longitudinal electronic dynamic dielectric function for a weakly correlated Fermi liquid-like phase for band electrons can be expressed as[28, 34]:

$$\epsilon^{-1}(\bar{q} + \bar{G}, \bar{q} + \bar{G}', \omega) = 1 + V_0(\bar{q} + \bar{G})\chi(\bar{q} + \bar{G}, \bar{q} + \bar{G}', \omega) \quad (28)$$

where  $\bar{G}$  and  $\bar{G}'$  are Umklapp vectors corresponding to the lattice background and in 2D [28, 23]

$$V_0(\bar{q} + \bar{G}) = \frac{2\pi e^2}{|\bar{q} + \bar{G}|} \quad (29)$$

is the bare Coulomb interaction between the electrons, projected in a 2D layer. At the RPA level  $\chi$ , the screened dynamic charge susceptibility neglecting the exchange-correlation effects, is given by [28, 33]:

$$\chi(\bar{q} + \bar{G}, \bar{q} + \bar{G}', \omega) = \frac{\chi_0(\bar{q} + \bar{G}, \bar{q} + \bar{G}', \omega)}{1 - V_0 \chi_0(\bar{q} + \bar{G}, \bar{q} + \bar{G}', \omega)} \quad (30)$$

where,  $\chi_0(\bar{q} + \bar{G}, \bar{q} + \bar{G}', \omega)$  is the free charge dynamic susceptibility given by the Lindhard function [28].

Hence, the effective static Coulomb interaction obeys the equation:

$$\frac{1}{V_{eff}(\bar{q} + \bar{G}', 0)} = -\chi_0(\bar{q} + \bar{G}, \bar{q} + \bar{G}', 0) + \frac{1}{V_0(\bar{q} + \bar{G})} \quad (31)$$

From eq.(31), one sees that  $(\frac{1}{V_{eff}} - \frac{1}{V_0})$  is proportional to the modulus of the static electronic Lindhard function,  $\chi_0(\bar{q} + \bar{G}, \bar{q} + \bar{G}', 0)$  being negative. This result will be used later in our analysis of the over-doped phase.

## 2.2 Comparison of our calculational results with experimental ones and those from other theoretical approaches

### 2.2.1 Under-doped regime (with strongly correlated nearest neighbour t-J model)

The effective Coulomb interaction ( $V_{eff}^{exp}$ ) in the long wavelength limit of the staggered magnetization can be extracted from the experimentally measured imaginary conductivity using the standard constitutive equations in the continuum limit [35]:

$$\epsilon'(\omega) = 1 - \frac{4\pi\sigma''}{\omega} \quad (32)$$

$$V_{eff}^{exp}(\omega) = \frac{V_0}{\epsilon'(\omega)} \quad (33)$$

leading to

$$V_{eff}^{exp}(\omega) = \frac{V_0}{1 - \frac{4\pi\sigma''}{\omega}} \quad (34)$$

where

$$\epsilon'(\omega) = 1 - \frac{4\pi\sigma''}{\omega} \quad (35)$$

with  $V_0$  being the bare Coulomb interaction,  $\epsilon'$  the real part of the dynamic dielectric function and  $\sigma''$  representing the imaginary part of the dynamic conductivity.

Many experiments have been carried out on the planes of lightly and optimally

doped  $\text{La}_{2-x}\text{Sr}_x\text{CuO}_4$ , including transmitted THz time-domain spectroscopy (THz-TDS) [27]. The effective Coulomb interaction is derived from the experimentally extracted imaginary conductivity in Table-I using the relation given above (see eq.(34)). In the table, we have used the bare onsite Coulomb interaction  $U=3.5\text{eV}$  in the undoped phase [27]. For extracting the bare Coulomb potential  $V_0$  of the itinerant doped phase in momentum space, ‘U’ has to be multiplied by an constant factor ‘c’.

Table 1: Real dielectric constant ( $\epsilon'$ ) and effective Coulomb interaction ( $V_{eff}^{exp}$ ) at  $\omega \rightarrow 0$  (i.e., static) and  $\tilde{q} \rightarrow 0$  (where  $\tilde{q} \equiv \bar{q} - (\pi/a, \pi/a)$ ) in the low to optimal-doping region, extracted from experimental results [27] (The on-site Coulomb interaction in the undoped phase is taken as 3.5eV [27]).

| $\delta$ | $\epsilon'$ | $V_{eff}^{exp}/c$<br>(in eV) |
|----------|-------------|------------------------------|
| 0.000    | 1.000       | 3.500                        |
| 0.070    | 0.999       | 3.503                        |
| 0.100    | 0.999       | 3.503                        |
| 0.120    | 0.999       | 3.503                        |
| 0.170    | 0.999       | 3.503                        |
| 0.225    | 1.000       | 3.500                        |

The experimentally extracted effective Coulomb interaction remains almost constant in the low and optimal-doping regime (shown in Table.1) [27]. This is in very good agreement with the behaviour of our theoretically obtained  $D_c$  in 2D (see Fig.(1)).

### 2.2.2 Over-doped regime

In this paper, we have studied the over-doped regime with three(3) different approaches, discussed earlier in details:

- (i) weakly correlated nearest neighbour t-J model
- (ii) weakly correlated t-J-like models with higher neighbour hoppings
- (iii) interacting high density electron gas and interacting band electrons

In the under-doped region we have compared our results with experimental results, but we did not get any suitable experimental results in the over-doped and highly over-doped regime. Hence, we will present here the comparison amongst the above theoretical approaches we have used.

We had derived an effective Coulomb interaction by using the dielectric function formalism for the lattice background (see eq.(31)). Now, taking a continuum approximation for simplicity, the corresponding Lindhard function in the  $\omega \rightarrow 0$  limit

takes the form[29]:

$$\chi_{2D}(q, 0) = -N(0)[1 - \Theta(\bar{q} - 2)\frac{\sqrt{q^2 - 4}}{q}] \quad (36)$$

where  $\theta$  is the heavy-side theta function with the property:

$$\theta(\bar{q} - 2) = 1 \quad \text{for } \bar{q} > 2 \quad (37)$$

$$\text{and} \quad \theta(\bar{q} - 2) = 0 \quad \text{for } \bar{q} < 2 \quad (38)$$

and  $\bar{q} = q/k_F$  [29]. Besides,  $k_F = \frac{\sqrt{2\pi(1-\delta)}}{a}$  (in 2D) and  $N(0)$  is the single fermionic density of states for one kind of spin at the Fermi circle. Hence from eqs.(36-38), it can be seen that the theta function goes to zero for  $q < 2k_F$  leading to  $\chi(q, 0) = -N(0)$ , which is a  $\delta$  independent constant value. This gives a discontinuous jump at  $q = 2k_F$ , followed by an increase in the value of  $\chi(q, 0)$  for  $q > 2k_F$ .

The doping concentration ‘ $\delta$ ’ and the wave vector ‘ $q$ ’ of the external electronic field/vector potential are independent quantities. However, corresponding to each  $\delta$ , there exists a value of  $q$  where  $\chi(q, 0)$  shows discontinuity. Let this be denoted by  $q_{dis}$ . Then  $q_{dis} = 2k_F$ . Since  $k_F = k_F(\delta)$ , one can determine  $\delta = \delta_{dis}$ , where a given  $q$  will assume magnitude  $2k_F$ . Obviously,

$$\delta_{dis} = 1 - \frac{q^2 a^2}{8\pi} \quad (39)$$

Since,  $\frac{1}{V_{eff}(q, 0)}$  varies linearly with the modulus of static Lindhard function (see eq.(31)), effective Coulomb interaction remains constant upto  $\delta_{dis}$  and the rise in the value of Lindhard function also manifests itself in the expression for  $V_{eff}(q, 0)$ . The region around  $\delta_{dis}$  refers to the regime of very high Coulomb interaction, which possibly indicates a tendency towards the formation of an itinerant charge density wave. Vojta and Sachdev have shown that a bond-charge ordering can occur in a t-J-like model in 2D at  $t=1.25J$  and the ordering wave vector  $q$  varies with  $\delta$  [4]. Using this variation, we find that the condition in eq.(39) is satisfied only with  $\delta \approx 0.18$  and hence the condition  $q = 2k_F$  is satisfied at  $\delta_{dis} \approx 0.18$ . The discontinuity in  $V_{eff}(q, 0)$  also shows up at this value of doping concentration [4].

The charge stiffness constant ( $\tilde{D}_c$ ) derived for pure t-J model with  $\alpha=0$  vanishes upto  $\delta \approx 0.61$  (for applied vector potential in the x-direction) as already discussed. As doping is increased further,  $\tilde{D}_c$  gives a non-zero contribution, resulting in the increase in value of the derived charge stiffness constant and the appearance of peak-like structure in the over-doped regime (see Fig.(1)). As we have stated earlier, only the nearest neighbour hopping is not sufficient for determining the charge correlations in the over-doped regime. By introducing two higher neighbour hoppings, one finds that the critical doping concentration ( $\delta_c$ ) shifts to the optimal doping region ( $\delta_c \approx 0.2$ ) (see Fig.(3)). This point  $\delta_c$  is very close to  $\delta_{dis}$  ( $\approx 0.18$ ) observed in  $V_{eff}$  calculated from the Lindhard function, as shown above.

Thus, we have established both qualitative and quantitative equivalences between derived  $D_c$  and  $V_{eff}$  in both under-doped and over-doped regimes in 2D. The sharp increase in  $D_c$  in the optimal doping region (with  $t_1-t_2-t_3-J$  model) implies a large enhancement of the magnitude of effective Coulomb interaction. This supports an approach to a charge ordering or the formation of an itinerant charge density wave, similar to one proposed in the Overhauser Theorem [29, 36].

### 3 Discussion

The generalized charge stiffness constants for 2D and 1D t-J-like models in strong and weak correlation limits are calculated. A weak dimensional dependence is seen for coupling between the mobile charge degrees of freedom. The charge coupling in the under-doped strongly correlated regime has been calculated by taking  $\alpha=1$  in the Gutzwiller state. The coupling in the over-doped weakly correlated Fermi liquid-like regime is derived by considering higher neighbour hoppings with a very small  $\alpha$  and also with  $\alpha=0$ , where the Gutzwiller state gets reduced to the ideal Fermi sea ground state. Our calculations bring out several important features and conclusions covering various aspects of correlated fermionic systems in low dimensions. These are discussed below in some details:

#### 3.1 Comparison between behaviours of $D_c$ and $D_s$ in 2D

The exchange energy contribution to  $D_c$  vanishes in the entire doping region (see eqs.(10)), resulting in the distinct behaviour of spin and charge stiffness constants [19, 20]. We have shown that  $D_c$  for two-dimensional lattice with pure t-J model remains zero throughout the lower doping region and exhibits a sharp rise at  $\delta=\delta_c=0.61$ . After this point,  $D_c$  immediately falls as doping is increased further (see Fig.(1)). The parameter  $\delta_c$  shifts to the optimal doping region when two higher neighbour hoppings are included (see Fig.(3)).

The region of enhanced Coulomb interaction around  $\delta_c$  may very well imply a tendency towards the formation of a charge density wave, as described in the previous section [29, 36]. Some of the previous theoretical results also confirms the presence of charge density wave states in the context of single-band t-J-U model [37]. Interestingly, the spin stiffness constant ( $D_s$ ) also shows a point of inflection (indicative of a possible phase transition) at the same  $\delta$ , where  $D_c$  exhibits the sharp rise [19]. Furthermore,  $D_c$  and  $D_s$  show almost identical behaviour for  $\delta > \delta_c$ , i.e. in the over-doped regime, which is a expected behaviour of Fermi liquid-like phases. In the under-doped regime however, the behaviour of the two stiffness constants are very different. Thus it can be concluded that the maximum around  $\delta_c$  separates the two regions of distinctly different behaviours. The regions are very likely to characterize (i) an anomalous conducting phase and (ii) a Fermi liquid-like metallic phase.

### 3.2 Comparison between behaviours of $D_c$ and $D_s$ in 1D

For t-J model, the quantity  $D_c$  in 1D vanishes at  $\delta=0$  and  $\delta \rightarrow 0$  and exhibits a maximum in the lower doping region. The peak shifts to further lower doping as the higher neighbour hopping amplitudes are increased and reaches the  $\delta \rightarrow 0$  limit at critical values of  $t_2$  and  $t_3$  (see Figs.(2),(4)). In a recent paper, we have shown that in one dimension,  $D_s$  displays a high value at  $\delta \rightarrow 0$  limit and falls rapidly with increase in doping concentration [20]. The drastic fall is immediately followed by the formation of a peak in the under-doped regime [20]. Hence, we see that  $D_s$  and  $D_c$  show completely distinct behaviour only in the very low doping region, whereas they show a similar trend as doping is slightly increased.

Furthermore, it is also seen that the tendency towards the formation of charge density wave occurs at much lower doping concentration in 1D than in 2D. Thus the dimensional dependence of charge stiffness in low dimensional systems is also established, similar to the spin stiffness case.

### 3.3 Equivalence of effective Coulomb interaction and generalized charge stiffness constant

The role of  $D_s$  as the effective exchange constant for the correlated doped magnetic systems was established using theoretical and other experimental results [19, 20]. Here in this paper, we have put forward our conjecture of establishing the role of  $D_c$  as the effective Coulomb interaction in doped antiferromagnets.

For 1D, we could not find any suitable experimental results in 1D chains to compare with our theoretical results. However, to prove our conjecture, we have compared our results in 2D with experimental results of  $\text{La}_{2-x}\text{Sr}_x\text{CuO}_4$  in the lower and optimal doping regime [27]. In the over-doped weakly correlated regime, we have presented a detailed comparison between  $D_c$  derived for the t-J-like models and the effective Coulomb interaction derived both for high density electron gas and interacting band electrons, as described in the previous section. The comparisons confirm the equivalence between the effective charge-charge coupling and our derived  $D_c$  both in the strongly and weakly correlated regimes in 2D.

In Fig.(5), we present a phase diagram of the doped antiferromagnets in 2D, based on their charge responses from the  $t_1-t_2-t_3-J$  model. We have shown the values of critical doping concentration ( $\delta_c$ ) for different values of  $t_3/t_1$  ratio, taking  $t_2/t_1$  as parameter. One can also notice that for a particular value of  $t_3/t_1$ , the transition between the two regions of different charge couplings, takes place at a lower value of doping concentration for higher values of  $|t_2/t_1|$ .

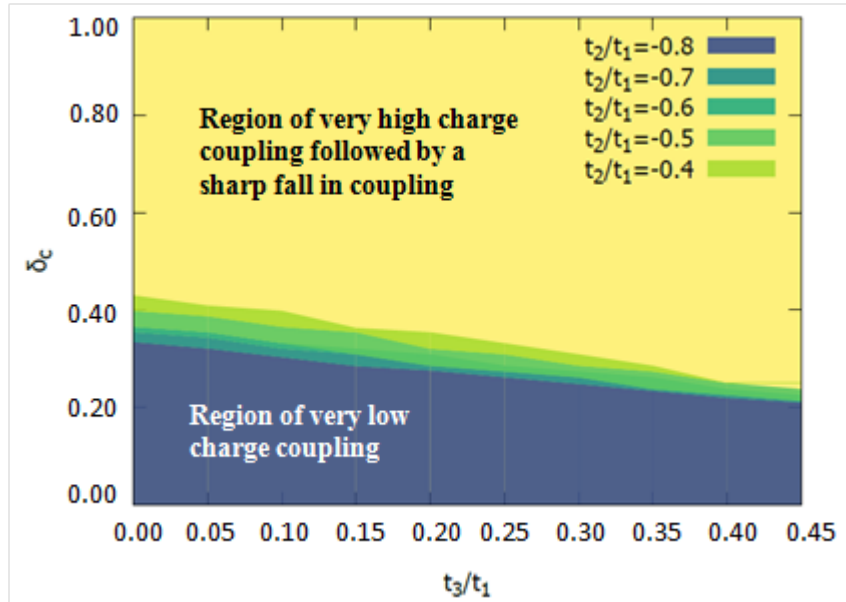


Figure 5: Phase diagram showing the critical doping concentration ( $\delta_c$ ), separating the regions of charge couplings, as a function of  $t_3/t_1$  (with  $t_2/t_1$  ratio as the parameter). The regions of doping concentration below  $\delta_c$  represent the regime very low charge coupling and above  $\delta_c$ , the interaction shows a very high value, followed by a sharp fall. The different colours are used for different ratios of  $t_2/t_1$  [ $\alpha=1$  has been taken].

### 3.4 Inadequacy of the t-J-like models in producing superconducting pairing of conventional type in low dimensional systems

In some of the recent works, real space pairing has been studied in the framework of the t-J-like models mostly in the under-doped phase [37, 38, 39]. In our calculation we do not get any region of negative charge stiffness, as is expected from the stability criteria (see eqs.(2)-(5)). Hence, the effective interaction between the mobile charge degrees of freedom never becomes attractive in these models and the reduction in magnitude of charge stiffness results in the decrease in effective Coulomb repulsion only. This reduction in effective Coulomb repulsion with increase in hole doping in turn gives rise to the enhanced possibility of fermionic pair formation in doped magnetic systems in 2D, provided some other attractive pairing mechanism is present. Thus we have established that the t-J-like models, on their own, can not produce Cooper pairing in q-space. This throws serious doubt on the feasibility of the momentum-space pairing based only on the t-J-like models as was advocated earlier [40, 41, 42, 43].

## References

- [1] D.Rybicki, M.Jurkutat, S.Reichardt, C.Kapusta, J.Haase, *Nature Communications* 7, 11413 (2016)
- [2] D.Chakraborty, C.Morice, C.Pépin, *Phy.Rev.B* 97, 214501 (2018)
- [3] K.V.Mitsen, O.M.Ivanenko, *Physics-Uspekhi* 60, 402 (2017)
- [4] M.Vojta, S.Sachdev, *Phy.Rev.Lett.* 83, 3916 (1999)
- [5] A.Aharony, R.J.Birgeneau, A.Coniglio, M.A.Kastner, H.E.Stanley *Phy.Rev.Lett.* 60, 1330 (1988)
- [6] R.J.Birgeneau, M.A.Kastner, A.Aharony, *Z.Phys. B: Cond. Mat.* 71, 57 (1998)
- [7] F.C.Zhang, T.M.Rice, *Phy.Rev.B* 41, 7243 (1990)
- [8] N.M.Plakida, R.Hayn, J.L.Richard, *Phy.Rev.B* 51, 16599 (1995)
- [9] N.M.Plakida, *Z.Phys.B* 103, 383 (1996)
- [10] G. Jackeli, N.M.Plakida, *Theor.Math.Phys.* 114, 335 (1998)
- [11] A.A.Vladimirov, D.Ihle, N.M.Plakida, *Phys.Rev.B* 80, 104425 (2009)
- [12] A.A.Vladimirov, D.Ihle, N.M.Plakida, *Phys.Rev.B* 83, 024411 (2011)
- [13] J.Kaczmarczyk, J.Spalek, T.Schickling, J.Bünemann, *Phy.Rev.B* 88, 115127 (2013)
- [14] D.J.Scalapino, “Handbook of High-Temperature Superconductivity”, edited by J.R.Schrieffer, J.S.Brooks, Chapter-XIII, Springer, NewYork (2007)
- [15] M.Ogata, M.U.Luchini, S.Sorella, F.F.Assaad, *Phys.Rev.Lett.* 66, 2388 (1991)
- [16] N.Kawakami, S.K. Yang, *Phys.Rev.Lett.* 65, 2309 (1990)
- [17] B.Sciolla, A.Tokuno, S.Uchino, P.Barmettler, T.Giamarchi, C.Kollath, *Phys.Rev.A* 88, 063629 (2013)
- [18] J.Sirker, A.Klümper, *Phys.Rev.B* 66, 245102 (2002)
- [19] S.Bhattacharjee, R.Chaudhury, *Physica B* 500, 133 (2016)
- [20] S.Bhattacharjee, R.Chaudhury, *J.Low Temp.Phys.* 193, 21 (2018)
- [21] R.Chaudhury, S.S.Jha, *Pramana* 22, 431 (1984)
- [22] D.Poilblanc, *Phy.Rev.B* 44, 9562 (1991)

- [23] J.Jaklič, P.Prelovšek, *Phy. Rev. B* 52, 6903 (1995)
- [24] E.Blackburn, J.Chang, M.Hücker, A.T.Holmes, N.B.Christensen, R.Liang, D.A.Bonn, W.N.Hardy, U.Rütt, O.Gutowski, M.V.Zimmermann, E.M.Forgan, S.M.Hayden, *Phy.Rev.Lett.* 110, 137004 (2013)
- [25] E.Dagotto, A.Moreo, F.Ortolani, D.Poilblanc, J.Riera, *Phy.Rev.B* 45, 10741 (1992)
- [26] N.M.Plakida, *Z.Phys.B* 103, 383 (1997)
- [27] D.Nakamura, Y.Imai, A.Maeda, I.Tsukada, *J.Phys.Soc.Jpn.* 81, 044709 (2012)
- [28] V.L.Ginzburg, D.A.Kirzhnits, “High-Temperature Superconductivity”, by chapter-III, New York: Consultants Bureau (1982)
- [29] G.F.Giuliani,G.Vignale, “Quantum Theory of the Electron liquid”, chapter-IV,V, Cambridge University Press (2005)
- [30] R.Chaudhury, *J.Phys.:Condens.Matter* 19, 496203 (2007)
- [31] J.Leshen, M.Kavai, I.Giannakis, Y.Kaneko, Y.Tokura, S.Mukherjee, W.C.Lee, P.Ayanjian, *Communication Physics* 2, 36 (2019)
- [32] T.Tohyama, Susumu Nagai, Yasumasa Shibata, Sadamichi Maekawa, *J.Low Temp. Phys.* 117, 211 (1999)
- [33] T.Tohyama, S.Nagai, Y.Shibata, S.Maekawa, *Phys.Rev.B* 82, 4910 (1999)
- [34] Y.A.Uspenskii, *Zh.Eskp.Teor.Fiz.* 76, 1620 (1979)
- [35] N.W.Ashcroft, N.D.Mermin, “Solid State Physics”, chapter-XVII, Harcourt College Publishers (1976), Preprint (2015)
- [36] A.W.Overhauser, *Phy.Rev.* 128, 1437 (1962)
- [37] M.Zegrodnik, J.Spalek, *Phy.Rev.B* 98, 155144 (2018)
- [38] J.Spalek, M.Zegrodnik, J.Kaczmarczyk, *Phy.Rev.B* 95, 024506 (2017)
- [39] J.Spalek, *Cond.Mat.Phys.* 11, 455-462 (2008)
- [40] V.Yu.Yushankhai, N.M.Plakida, P.Kalinay, *Physica C* 174, 401 (1991)
- [41] Kazuhiko Sakakibara, Ikuo Ichinose, Tetsuo Matsui, *Phys.Rev.B* 46, 14779 (1992)
- [42] N.M.Plakida, V.S. Oudovenko, P.Horsch, and A.I.Liechtenstein, *Phy.Rev.B* 55, R11997(R) (1997)
- [43] R.Chaudhury, *Theor.Math.Phys.* 136, 1022 (2003)